Jet installation noise reduction using porous treatments

Hasan Kamliya Jawahar[a,*], Sergey A. Karabasov[b,**], Mahdi Azarpeyvand[a,]

[a]*Department of Aerospace Engineering, University of Bristol, Bristol BS8 1TR, UK*
[b]*School of Engineering and Material Science, Queen Mary University of London, Mile End Road, London, E1 4NS*

Abstract

The possibility of jet-installation noise reduction has been experimentally demonstrated using a flat-plate fitted with flow permeable metal foam fitted at the trailing-edge. Tests were conducted for single stream cold subsonic jets with a round nozzle adjacent to a flat-plate for a wide range of flow velocities ($M = 0.3-0.9$) in an anechoic chamber. Thorough investigations of the far-field noise for various polar angles were carried out to demonstrate the regions with noise reduction. Four porous trailing-edges were tested with various increasing permeability and surface roughness. Far-field results showed substantial noise reduction for the installed configuration fitted with porous trailing-edges. Overall sound pressure level scaling with velocity demonstrates that trailing-edge scattering noise is reduced by the application of from porous trailing-edge. Detailed analysis using coherence and correlations of the far-field results are also presented to gain a better understanding of the effects of different porous materials. The effect of plate distance was also investigated and the results showed tonal characteristics for cases with high surface roughness. Overall, a thorough experimental study is provided for understanding the jet installation noise reduction mechanism using porous trailing-edges.

Keywords: Aeroacoustics, Jet noise, porous materials, jets installation, jets.

*Corresponding Author, Research Associate, Department of Aerospace Engineering
**Professor of Computational Modelling, School of Engineering and Material Science
Professor in Aeroacoustics, Department of Aerospace Engineering
Email addresses: hasan.kj@bristol.ac.uk (Hasan Kamliya Jawahar), s.karabasov@qmul.ac.uk (Sergey A. Karabasov), m.azarpeyvand@bristol.ac.uk (Mahdi Azarpeyvand)

1. Introduction

Noise generated as a result of the interaction between the exhaust flow of a jet and an airframe surface present at close proximity is referred to as Jet Installation Noise (JIN) following the early works of Bushell [1], Head and Fisher [2], and more recent publications [3, 4]. In addition to the presence of turbulence-mixing noise in installed subsonic jets, additional noise sources have been identified at the surface of the trailing-edge especially at low and mid-frequencies in the direction upstream to the jet [2, 5–8], which in some cases can also lead to the generation of tones [9, 10]. The hydrodynamic pressure waves, generated in the mixing layer of an isolated jet are evanescent in comparison to the acoustic waves propagating to the far-field. However, the presence of high-lift devices, which are drawn closer to the jet plume during take-off and approach intensifies Jet Installation Noise by scattering the hydrodynamic pressure by the wing trailing-edge to the far-field noise [11]. Computational studies based on the eddy-resolving approaches have shown that installation effects can amount to approximately 4EPNdB of the acoustic footprint of the jet [12]. With the introduction in ultra-high bypass ratio engines, these additional noise sources are set to become even more important as the distance between the jet and airframe progressively decreases [13]. Several attempts have been made to understand the detailed mechanisms behind this phenomenon in order to mitigate the additional noise, which depends on the distance between the jet and the scattering surface. For example, Mengle et al. used tailored chevron nozzles to reduce the installation effects of jet, however, the application of chevrons was not sufficient to completely mitigate the jet noise due to interaction with the trailing-edge [14].

Notably, the use of porous materials on the scattering surface may offer a solution to effectively mitigate the trailing-edge noise. The material properties like porosity and permeability can be manipulated to help reduce the trailing-edge noise by maintaining the pressure balance between the pressure and suction sides of the airfoil trailing-edge [15, 16]. Previous experimental evidence suggests that the application of porous materials may reduce the flap side-edge noise when compared to an untreated one [17]. In application to the turbulent boundary-layer trailing-edge noise, Sarradj and Geyer [15] reported a reduction of up to 10 dB by applying a fully porous SD7003 airfoil. The benefits of porous treatments for airfoil noise application may not always be achieved for all frequencies. For example, the acoustic beamforming results by Rubio-Carpio et al. [18]. showed the trailing-edge noise reductions of up to 10 dB in the low and mid-frequency regions but an increase for high frequencies [18]. In this case, the dominant noise source location moved to the permeable surface upstream of the trailing-edge with porous inserts on 20% of the chord as a consequence of the modified turbulence intensity, shear stress in the boundary layer, and radiation efficiency at the edge induced by the porous treatment [19].

In a recent study, Rego et al. [20], successful demonstrated jet installation noise reduction of up to 10 dB with the use of metal foam and a perforated trailing-edge at low jet velocities. It was hypothesized that the noise reduction occurred as a result of permeability effects mitigating the pressure imbalance between the upper and lower sides of the plate. In a recent numerical study, Rego et al. [21] showed that the noise reduction in porous materials occurred due to the suppression of the scattering effects at the trailing-edge. Moreover, the dominant acoustic source was identified at the solid-permeable junction for the trailing-edge treated with porous materials.

Although recent studies [20, 21] have shown that the use of porous trailing-edges can result in the reduction of jet-installation noise, key factors such as the effects of porosity and permeability on the level of noise reduction are yet to be fully characterized. Therefore, the present study aims to fill the knowledge gap in the literature by investigating the effects of porosity and permeability on jet-installation noise. An additional novelty in this study is the demonstration of the possible detrimental effects such as tonal behavior for jet-installation noise with the use of porous treatments. In the present study, a systematic experimental investigation for jet-installation noise was conducted using four different metal foam trailing-edges with different porosity and permeability properties for a wide range of acoustic jet Mach numbers, 0.3-0.9. Far-field acoustic measurements for a range of jet-plate distances are reported and the results are discussed in conjunction with the existing jet noise literature.

2. Experimental setup

The experiments were conducted in the newly commissioned Bristol Jet Aeroacoustic Research Facility (BJARF) at the University of Bristol. As shown in Fig. 1, the flow in BJARF is conditioned and silenced using three different custom-built in-line silencers to create a clean quiet flow at the jet exit. The first two silencers with a volume of 93 liters each are placed right after the control valve outside the anechoic chamber and have a diameter of 0.3 m and a height of 1.5 m each. The third large silencer with a volume of 260 liters is placed inside the anechoic chamber and has a diameter of 0.457 m and a height of 1.9 m. The silencers are equipped with perforated tubes for the flow with the remaining area packed with glass wool. The anechoic chamber where the tests were carried out has dimensions of 7.9 m in length, 5.0 m in width, and 4.6 m in height, including the surrounding acoustic walls [22]. The silencers, the collector, and the far-field array are covered with foam prior to testing. The acoustic Mach number and the flow conditions are determined from the total temperature and pressure probes placed within the large silencer and in the acoustic chamber. The jet installation study was carried out using an unheated round jet and a rigid flat-plate placed at different proximity to the jet stream, as shown in Figs. 2 and 3. For the round jet, SMC000 nozzle was used which has been well characterized by Bridges and Brown [23] for isolated configuration. In the present study, the tested nozzle is a 3:1 down-scaled version of the nozzles used by Bridges and Brown [23], corresponding to an exit jet diameter of $D = 16.933$ mm. The tests were carried out for a wide range of subsonic flows with acoustic Mach number ranging from M = 0.3 to 0.9. The flat-plate used in the present experiment was made from a 5 mm thick perspex material. The plate had a total length of $10D$ and a total span of $S = 30D$ to avoid side-edge scattering. The flat-plate was mounted on an automated traverse system with the capability to move in the radial direction. As shown in Figs. 2 and 3, the tests were carried out for a flat-plate of length $L = 6.5D$ (between the nozzle lip and the trailing-edge) and for various plate heights $H = 1.7D, 2D, 2.5D, 3D, 3.5D$, and $4.5D$, placed radially away from the jet centerline. Physical constraints in the experimental setup restricted the testing of plate heights lower than $H < 1.7D$. The results are presented for a plate height of $H = 2D$ to avoid flow interaction on the plate surface and trailing-edge as this could produce additional noise sources related to flow impingement and scrubbing. This study concerns the investigation of the linear-hydrodynamic pressure field with the trailing-edge, therefore plate heights with flow interaction were not considered. The plate

extends $3.5D$ upstream from the nozzle exit to avoid scattering effects at the leading edge as it was also limited by nozzle geometry. A recent study [20] showed that the effect of streamwise extent of porous trailing-edge had a minimal influence on the far-field spectra of jet-installation noise. It was also demonstrated [20] that the porous treatment of a small section in the streamwise extent ($\approx 1D$) is sufficient for achieving noise reduction. Therefore, in the present study, porous treatments of length $L_p = 1.5D$ were fitted on a flat-plate with interchangeable trailing-edges extending full span. A solid trailing-edge referred to as baseline was tested along with four different types of porous metal foams named based on the pores per inch (PPI)– 80PPI, 45PPI, 35PPI, and 25PPI, as shown in Fig. 4 and Table 1. It is important to note that the porous trailing-edge treatments had a thickness (5 mm) identical to that of the flat-plate it is mounted on.

Far-field noise measurements were acquired using an array of 18 microphones distributed on an arc in the axial direction centered on the jet exit at a distance of 1.6 m (94.49D) that covered inlet angles between $\theta = 60°$ upstream and $\theta = 155°$ downstream with the $\theta = 90°$ microphone positioned right above the nozzle exit. Measurements were acquired using a 1/4-inch G.R.A.S 40PL microphone with corrected flat frequency response at frequencies from 10Hz to 20 kHz, and a dynamic range of 150 dB. An additional 1/8-inch G.R.A.S 46DD microphone with a flat frequency response of up to 100 Khz was also placed at $\theta = 90°$ for cross-checking the results. The data were acquired using a National Instrument PXIe-4499 for $t = 24$ s at a sampling frequency of $f = 2^{17}$ Hz. The power spectrum results were obtained using the power spectral density (PSD) of the pressure signals with the Hanning window and the acquired data were averaged 220 times to yield a frequency resolution of $\Delta f = 2$ Hz. The sound pressure level (SPL) spectrum can then be calculated from $SPL = 20{\cdot}log_{10}\,(p_{rms}/p_{ref})$, where p_{rms} is the root-mean-square of the acoustic pressure and $p_{ref} = 20\ \mu$Pa is the reference pressure. The sound pressure level of the acoustic pressure signal is corrected to a reference distance of 100D. The SPL was corrected using an atmospheric attenuation function to account for the sound absorption through the atmosphere [24, 25].

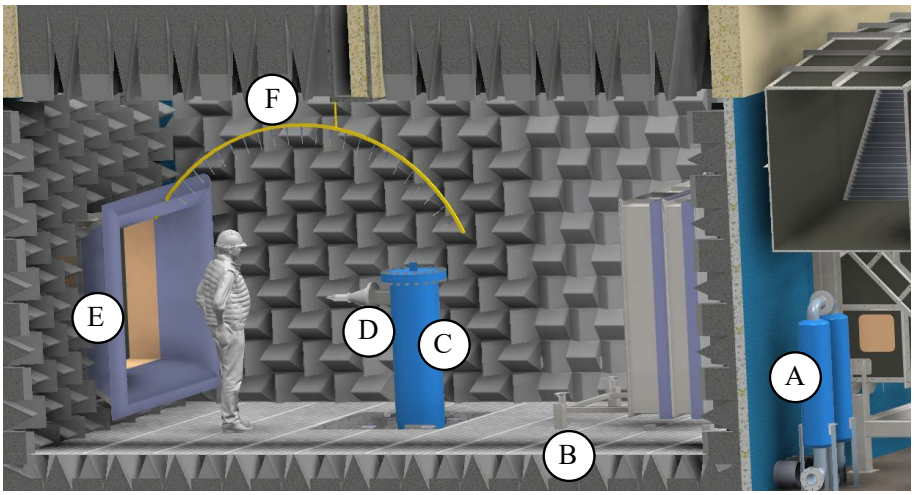

Figure 1: Side view of the aeroacoustic facility including the silencers: (A) First and second silencer, (B) Connecting underground pipe, (C) Third large silencer, (D) Contraction for the jet nozzle, (E) Collector, and (F) Far-field microphone array.

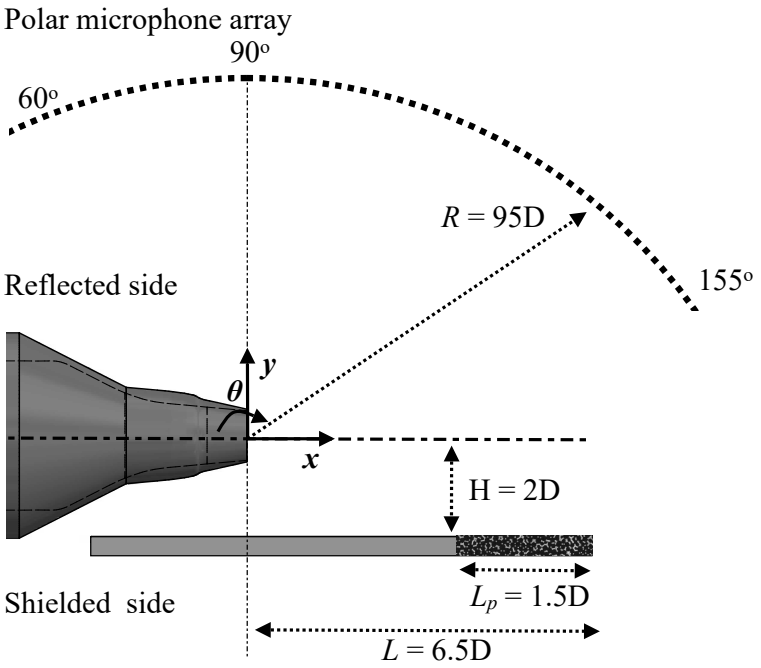

Figure 2: Schematic of the experimental setup with the position of the far-field microphones used in the present study.

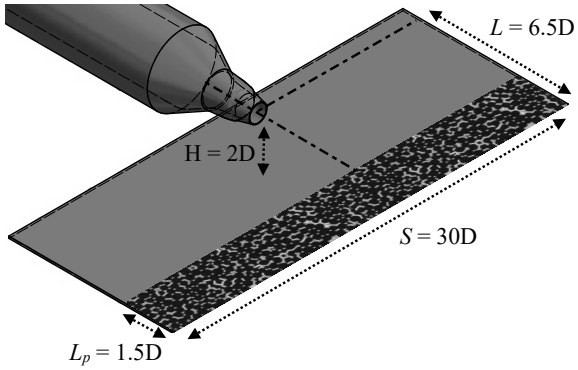

Figure 3: Isometric view of the experimental setup showing the porous length, plate length, span and height.

3. Porous materials

Four different open-cell uncompressed Nickle metal foams with different macroscopic parameters are chosen for the current study. The porous metal foams were chosen over other options because of its superior trailing-edge noise reduction properties shown in the previous studies [26–29]. The porous metal foams are commercially available and are manufactured by XINDA through electrodeposition of pure Nickle on polyurethane foam. The considered metal foams are of a rigid structure with regular round pores, which are characterized by the pore size, i.e., pores per inch (PPI) namely, 80PPI, 45PPI, 35PPI, and 25PPI (see Fig. 4). Notably, the effectiveness of porous materials as a flow control technique is known to strongly depend on their porosity and permeability coefficients. The coefficients of porosity,

Table 1: Properties of the metal foams used in the present study.

Foam	Porosity, φ (%)	Permeability, κ ($\times 10^{-8} m^2$)	Mean roughness, Ra (μm)
80 PPI	74.76	0.7688	211.752
45 PPI	85.37	2.0557	1760.869
35 PPI	88.39	4.4166	1791.044
25 PPI	90.92	8.1934	1922.279

φ (the ratio of the pores' volume to the overall volume) and permeability, κ (the coefficient in Darcy's law corresponding to the capacity of flow to permeate through a porous medium) of the considered metal foams are summarised in Table 1. Additionally, the average roughness properties of the foam, which corresponds to the mean pore size (Ra) for each of the considered porous metal foams has been included in the same table. It is evident that the surface roughness increases with the increase in the porosity of the metal. The aerodynamic and acoustic characteristics of these metal foams are documented in detail in previous studies [26–29]. Porosity and permeability of the trailing-edge treatments were shown to significantly affect the aerodynamic characteristics. Porous treatments showed improved drag performance compared to the solid configurations. However, amongst the tested porous configurations, the highest levels of drag were found for cases with high levels of porosity and surface roughness. The 80PPI case with the lowest levels of porosity and surface roughness was found to produce the least amount of drag compared to all the tested cases.

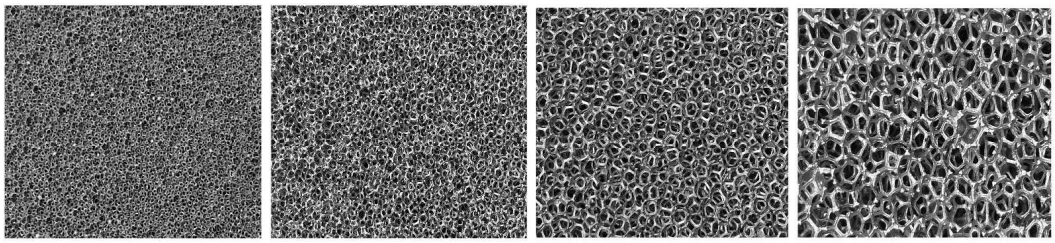

(a) Porous 80PPI (b) Porous 45PPI (c) Porous 35PPI (d) Porous 25PPI

Figure 4: Photographs of the metal porous materials used in the present study.

4. Results and Discussion

4.1. Far-field noise validation

As the first step, in order to gain confidence in the experimental setup, the far-field noise measurements for the isolated configuration for a round nozzle with a jet diameter of $D = 16.93$ mm is compared with the reference jet noise data set from NASA [30]. The far-field measurements are compared at various inlet angles (θ), and the results are presented in Fig. 5 for a Reynolds number of $Re = 196,000$, calculated based on the jet diameter $D = 16.93$ mm. Notably, the far-field measurements of the current experimental setup are in good agreement with the reference noise spectra corrected for the distance and diameter.

It should be noted that, due to the scaled-down size of the current nozzle, the results are presented only up to $St = 2$, where St is the Strouhal number based on the jet nozzle exit diameter and jet velocity at the nozzle exit ($St = fD/U_j$). This Strouhal number range is deemed sufficient since the present study is concerned with the jet installation effect, which peak lies well below $St = 1$.

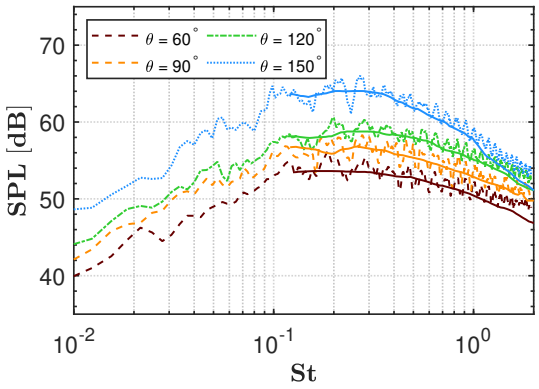

Figure 5: Comparison of SPL for isolated round convergent nozzle configurations with the experimental data set from Brown and Bridges et al. [30] (solid lines) at different polar locations ($\theta = 60°, 90°, 120°$ and $150°$) obtained at $M = 0.5$ corresponding to a Reynolds number of $Re = 196,000$.

4.2. Far-field pressure measurements

Results of the Sound Pressure Level (SPL) measurements on the reflect side corrected to a distance of 100D for the porous trailing-edge configurations with 80PPI, 45PPI, 35PPI, and 25PPI are presented in Figs. 6 to 9 for acoustic Mach number $M = 0.3 - 0.9$. The results are presented for four locations, namely, upstream inlet location $\theta = 60°$, slide line location $\theta = 90°$, and downstream locations $\theta = 120°$ and $150°$. For the isolated jet cases, an increase in peak noise levels in the order of ≈ 34 dB was found between the lowest and highest acoustic Mach numbers ($M = 0.3 - 0.9$) at $\theta = 90°$. This is in excellent agreement with Lighthill's scaling law, U_j^8 for jet mixing noise spectra [7], and which is also in agreement with previous jet noise experiments [2]. For all installed jet cases at Mach numbers $M = 0.3$ and 0.5 (Figs. 6 and 7), a significant spectral hump appears at the frequencies around $St = 0.1$, which completely dominates over the jet mixing noise spectra. The peak is due to the installation effect and swiftly disappears for higher frequencies starting from the characteristic frequency of isolated jet noise ($St = 0.2$). As the jet velocity is further increased to $M = 0.7 - 0.9$ (Figs. 6 and 9), the spectral hump representative of the installation effect diminishes compared to the background jet mixing noise spectra. This is in line with the previous studies [2, 8] which showed that for high-speed jets, $St > 0.7$, the spectra for the installed jet cases are dominated by quadrupole noise sources representative of jet mixing noise. [31].

For relatively low Mach numbers, $M = 0.3$ and 0.5 (Figs. 6 and 7), noise reduction in the range of 3-4 dB was found between $St = 0.02 - 0.2$ for all the porous configurations in comparison with the baseline case. This confirms that the application of flow-permeable materials to the trailing-edge reduces the noise generated by scattering of the near-field hydrodynamic waves at the trailing-edge. The noise reduction is due to the alteration of the scattering on the porous trailing-edge surface, which effect has also been discussed recently by Rego et al. [32].

The results for the baseline jet installation case at $\theta = 60°$ show noise reduction in the low-frequency range $St < 0.07$ of about 1-2 dB compared to the noise spectrum $\theta = 90°$. This could be attributed to the dipolar directivity pattern, which is known to have the maximum energy radiated in the direction normal to the scattering surface. However, for the mid-frequency range $St = 0.2 - 0.3$, there is a further increase for aft inlet angles $\theta = 60°$ in comparison with the sideline observer location, $\theta = 90°$. The difference between the scattering effects at low and low frequencies can be attributed to non-compact source interference effects when the size of the trailing-edge noise source becomes comparable to the acoustic wavelength. For the porous cases, the noise radiated in the direction upstream to the jet at $\theta = 60°$ shows a reduction of about ≈ 2 dB in the mid-frequency range $St = 0.2 - 0.3$ in comparison with the baseline case. This primarily occurs as a result of the altered scattering of the hydrodynamic field due to the porous surface treatment. Similar to the baseline installation case, the noise spectra of the porous cases at $\theta = 90°$ for low frequencies, $St = 0.1$ show amplification in comparison with the lower inlet angle in accordance with the dipolar directivity pattern. At $\theta = 150°$, which corresponds to the peak jet noise directivity, an increase in noise of up to 10 dB is found in all cases compared to the upstream direction apart from the $M = 0.3$ jet. For noise spectra results of the porous cases at $\theta = 150°$, a spectral hump with reduced energy compared to the baseline is found at $M = 0.3$ and 0.5. In line with the observations for the sideline noise spectra, for $M = 0.7$ and 0.9, the results of the porous cases follow the same trend as the baseline case since the scattering effect in the downstream jet flow direction is weak. It is also worth noting that the highest noise levels in all the presented cases are found at $\theta = 150°$. Those highest levels are attributable to the jet installation mechanism only for the slowest jet case, $M = 0.3$.The 45PPI configuration follows a trend similar to the 80PPI configuration at $M = 0.3$ with noise amplifications of about 4 dB in low frequencies between the upstream and downstream directions. A small tone is observed in the mid-frequency region for all the tested configurations at $St = 0.2-0.3$. However, these tones were completely absent for the baseline installed jet configuration for all the considered Mach numbers ($M = 0.3 - 0.9$). These tones arise only for the porous configurations, and the magnitude of the tones increases as the porosity coefficient increases. Notably, in the case of 25PPI, two tones are observed in the mid frequencies at $St = 0.2$ and $St = 0.3$ for $M = 0.5 - 0.9$, and at all inlet angles. The magnitude of the tone noise was also found to increase with increasing Mach number. These observations suggest that large pore sizes of the metal foam may trigger the acoustic feedback mechanism between the thin shear layers at the jet inlet, which is most susceptible to the linear hydrodynamic instability and the effective impedance condition on the porous metal foam. It could also be hypothesized that the junction between solid and flow-permeable surfaces acting as the dominant noise source might be triggering the acoustic feedback mechanism, particularly for cases with high permeability. Although the porous trailing-edges provide noise reduction, cases with high porosity and permeability result in unfavorable tonal behavior. This tone appears to be highly dependent on the plate height and will be discussed in detail in Sec. 4.6.

For completeness, the Overall Sound Pressure Level (OASPL) results of various permeable porous metal foams measured at microphone locations from $\theta = 60°$ up to $\theta = 155°$ at $M = 0.3 - 0.9$ integrated in the range $0.02 < St < 3$ are shown in Fig. 10. The OASPL are presented in the same manner as the previous noise spectra with 60° corresponding to the upstream direction and 155° being in the downstream direction closer to the jet axis

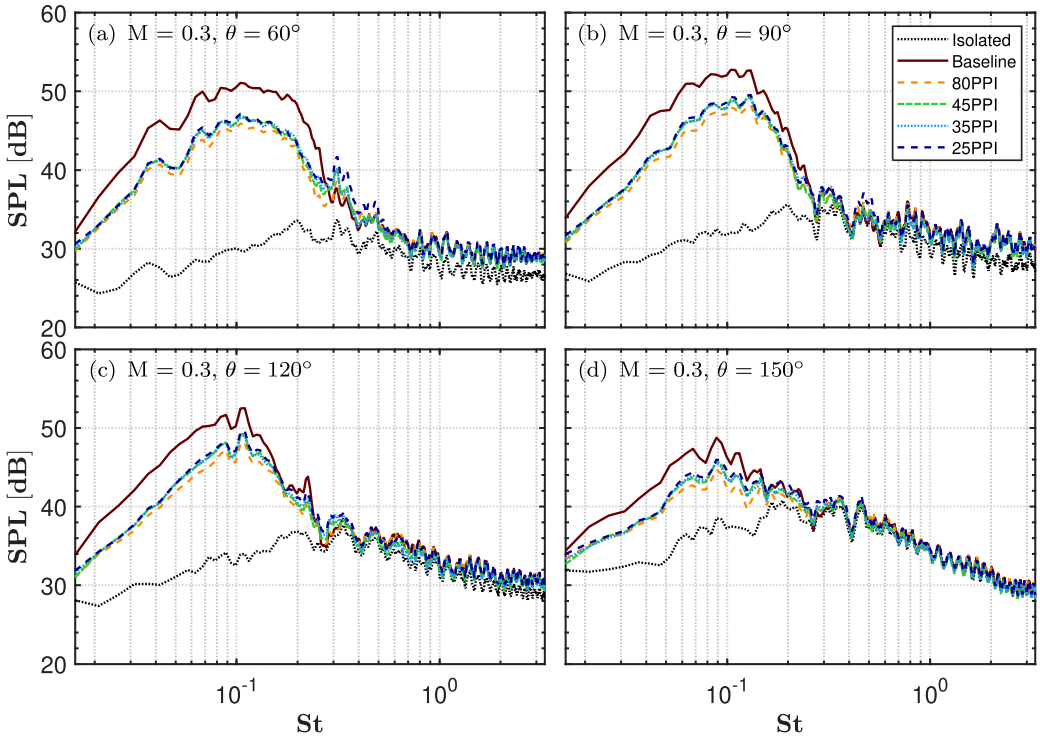

Figure 6: Sound pressure level at 100D for various inlet angles $\theta = 60°, 90°, 120°$ and 150° at $M = 0.3$.

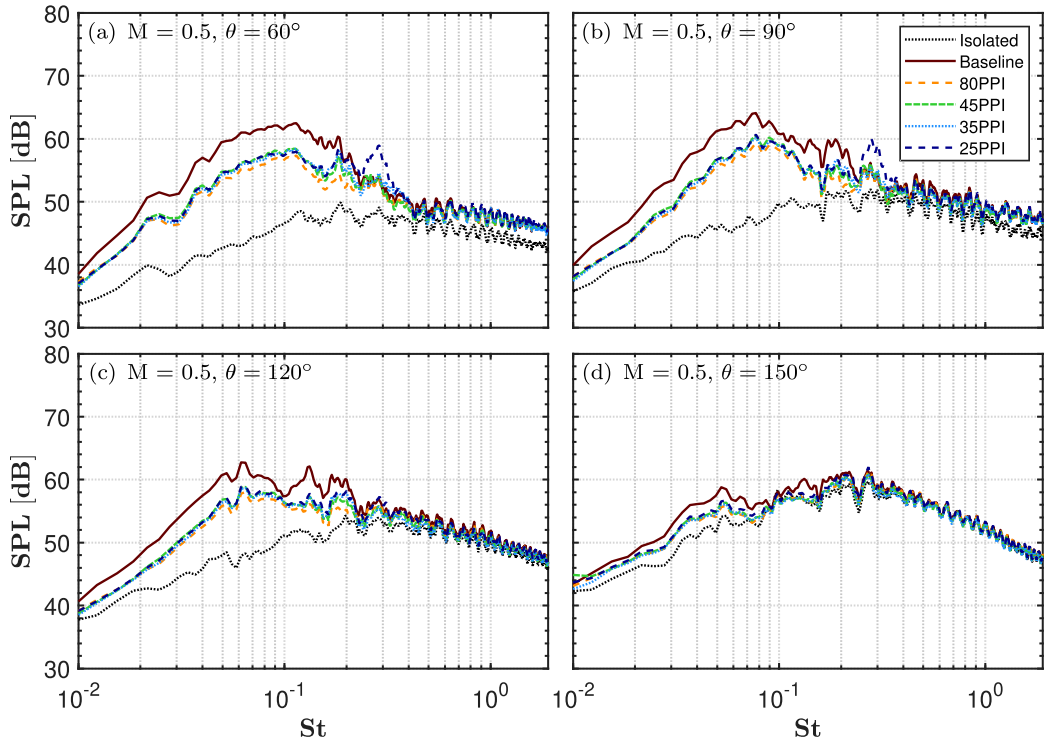

Figure 7: Sound pressure level at 100D for various inlet angles $\theta = 60°, 90°, 120°$ and 150° at $M = 0.5$.

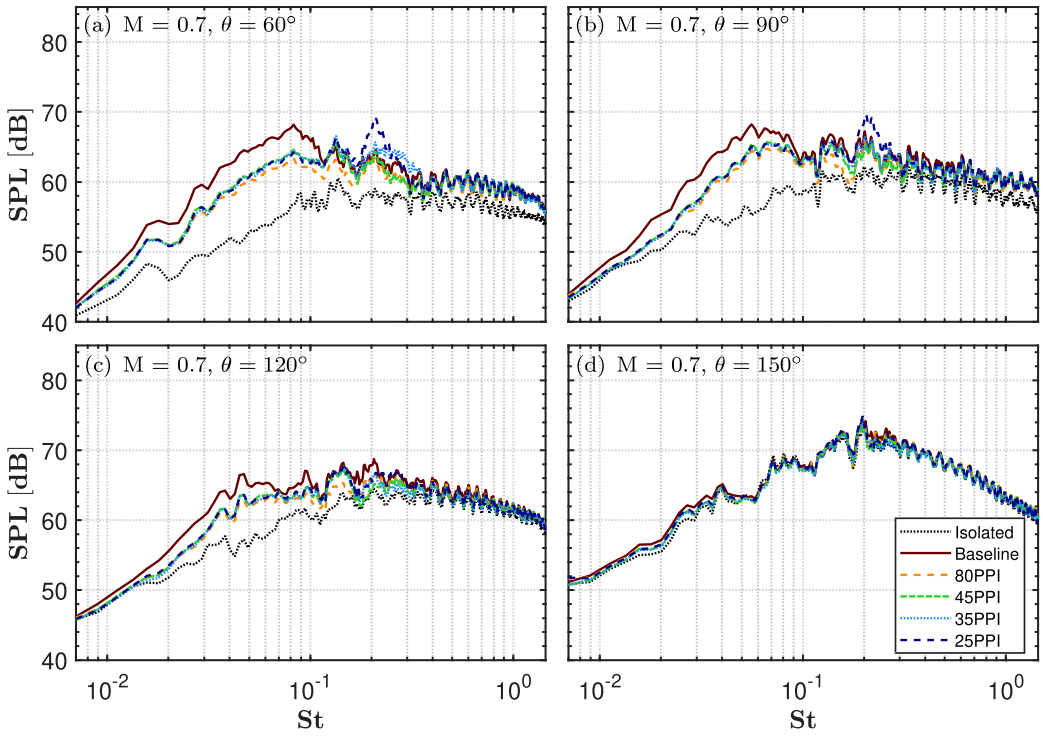

Figure 8: Sound pressure level at 100D for various inlet angles $\theta = 60°, 90°, 120°$ and 150° at $M = 0.7$.

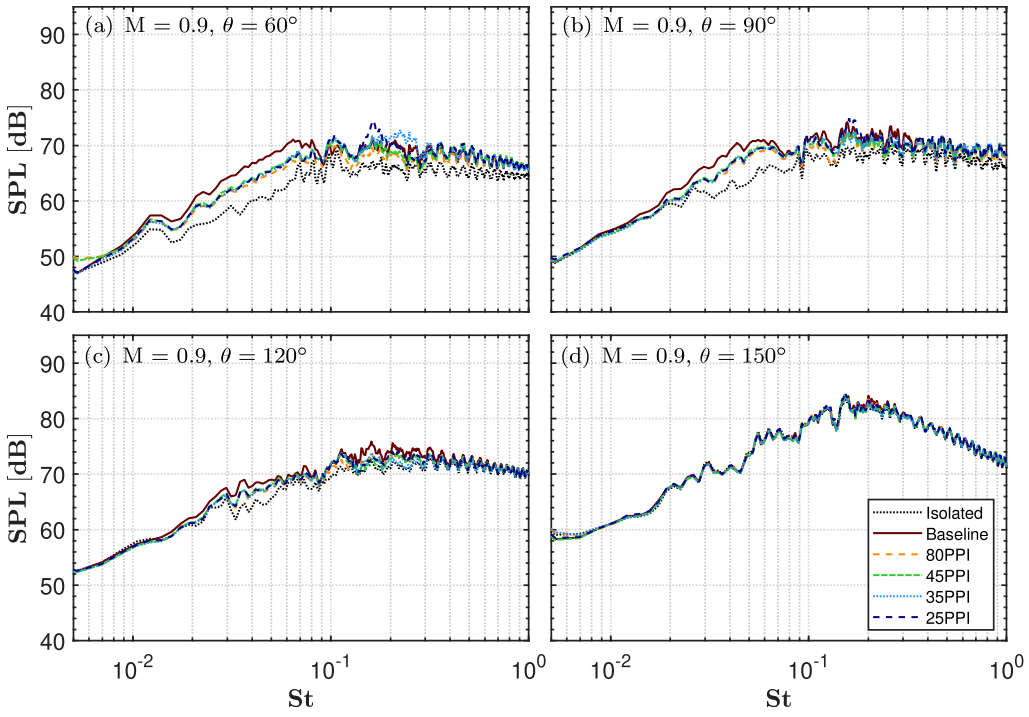

Figure 9: Sound pressure level at 100D for various inlet angles $\theta = 60°, 90°, 120°$ and 150° at $M = 0.9$.

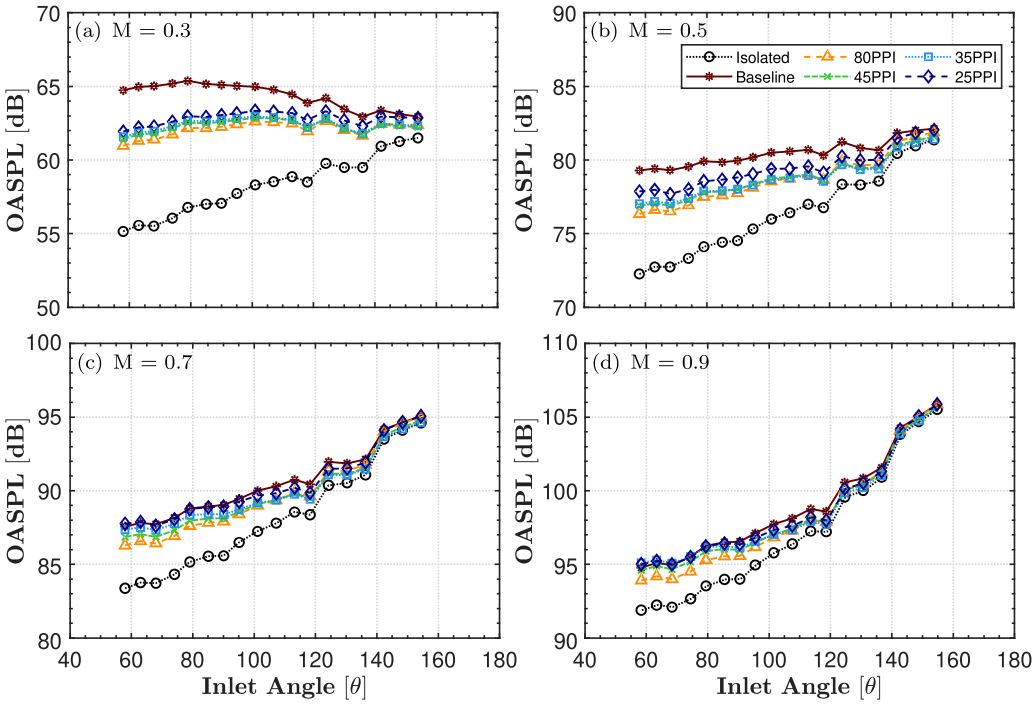

Figure 10: OASPL for the various trailing-edge treatments at various inlet angles $60° - 155°$.

(Fig. 2). The OASPL of the installed jet configurations is substantially higher in the upstream and sideline jet directions in comparison with the isolated jet, which is consistent with the cardioid directivity of jet installation noise as proposed by Ffowcs-Williams Hall [33] and the previous noise spectra observations. This behavior is consistent with noise scattering from a plate trailing-edge. At low Mach number $M = 0.3$ there is an increase of ≈ 10 dB in the OASPL calculation for the installed configurations compared to the isolated jets at upstream angles. The flow permeable porous metal foams show considerable noise reduction for the installed configuration at low Mach number $M = 0.3$. The largest noise reduction happens at 80PPI with ≈ 4 dB and the smallest noise reduction corresponds to 25PPI with ≈ 3 dB compared to the baseline. The results show a difference between the porous foam treatments and the baseline only for inlet angles ranging from $\theta = 60°$ to $130°$, with the highest noise reduction seen at lower inlet angles, thereby reaffirming that the noise reduction for the porous materials is achieved due to reduction in scattering effects. This reduction could be due to the suppression of the dipole noise sources at the trailing-edge for the porous treatments. As the jet velocity is increased to $M = 0.5$ the difference in OASPL between the baseline and isolated cases decreases from ≈ 10 dB to about ≈ 7 dB at upstream axial locations. Similar to $M = 0.3$ the results for $M = 0.5$ show the largest noise reduction for 80PPI of up to ≈ 3 dB and the lowest noise reduction for 25PPI of about ≈ 1 dB compared to the baseline case. It is noteworthy that the 45PPI and 35PPI configurations showed similar levels of noise reduction and performed better than 25PPI. This poor performance of 25PPI could be attributed to the additional tone observed in the mid-frequency range. At high Mach numbers $M = 0.7$ and 0.9, the difference in OASPL between the baseline installed and the isolated jet cases is about ≈ 4 dB and ≈ 3 dB, respectively. At low inlet angles, the

only porous configuration that showed noise reduction is 80PPI with a reduction of up to $\approx 1-2$ dB. Notably, at inlet angles $\theta > 120°$ the noise difference between the installed and isolated configurations is very small. These results show that the noise at observer positions closer to the jet axis in the downstream locations is dominated by the turbulence-mixing noise [34], indicating that the turbulence-mixing component is unaffected by the presence of the plate and porous treatments. Overall, the OASPL results reconfirm that for the upstream inlet angles ($\theta < 90°$) the noise is dominated by the trailing-edge scattering, and thus the use of porous trailing-edges can result in the reduction of installation effect noise. In the downstream locations ($\theta > 120°$), the installation effect due to the scattering from the trailing-edge is not dominant in comparison with turbulence-mixing noise, therefore, for the peak jet noise angles, the total noise shows little sensitivity to the porous edge treatment.

4.3. Coherence between shielded and reflected side

Following several studies in the literature [8, 31, 35], the present study has hypothesized that the observed low-frequency noise amplification is due to the scattering of the near-field hydrodynamic waves by the trailing-edge. This hypothesis can be verified by analyzing the pressure signals from microphones placed on both sides of the trailing-edge, e.g. the reflected side $\theta = 90°$ versus the shielded side $-90°$. The coherence function between the two sideline microphones placed on the shielded and reflected side was calculated using

$$\gamma^2_{p_s p_r}(f) = \frac{\mid \Phi_{p_s p_r}(f) \mid^2}{\Phi_{p_s p_r}(f)\Phi_{p_s p_r}(f)} \tag{1}$$

where p_s denotes the microphone location on the shielded side and p_r is the microphone on the reflected side. The coherence of the pressure signals was calculated with the Hanning window and the acquired data were averaged 800 times to yield a frequency resolution of $\Delta f = 31$ Hz. To further improve the smoothness of the coherence spectra, Savitzky-Golay filtering with a third order polynomial was used with a frame length of 11. It should be noted that special attention was paid in order to maintain the key spectral characteristics of the coherence when applying the noise filter. Figure 11 compares the SPL on the shielded and the reflected side at $\theta = \pm 90°$ for the baseline installed configuration with the isolated jet at the same acoustic Mach number, $M = 0.3$. The dipole nature of the trailing-edge noise results in a prominent low-frequency hump for frequencies $St < 0.3$ on both the shielded and reflected sides. For higher frequencies, at $St > 0.3$, the reflected side receives more noise compared to the shielded one in accordance with the high-frequency jet noise propagation which is enhanced on the reflected side of the surface. Indeed, the high-frequency jet noise sources are located over the first few jet diameters downstream of the nozzle exit, in which part of the jet is shielded by the flat-plate. The noise from these sources is further amplified due to the reflection from the trailing-edge. Accordingly, the differences between the noise spectra on the reflected and the shielded side become more notable at high frequencies ($St > 1$) where the propagation effect is expected to be more important compared to the low frequencies. The current observations are in line with Brown [4], who found that the reflected side of the jet shows an increase of 3 dB in SPL in comparison with the isolated jet.

The normalized coherence results for different jet Mach numbers corresponding to the tested configurations are further presented in Fig. 12. Compared to the isolated jet case, the coherence for the installed configuration is notably higher, $\gamma^2_{p_s p_r} > 0.8$ for $M = 0.3$ and 0.5

(compared with $\gamma^2_{p_s p_r} = 0.4 - 0.6$ for the isolated case) , and $\gamma^2_{p_s p_r} = 0.6 - 0.8$ for $M = 0.7$ (compared with $\gamma^2_{p_s p_r} = 0.2 - 0.4$ for the isolated case, respectively). Furthermore, for the peak installation noise frequencies, St 0.1 and $M = 0.3 - 0.5$ (see Figs. 6-9) the coherence of the installed jet cases reaches high values $\gamma^2_{p_s p_r} = 0.9$. The high levels of coherence are in line with the previous studies [11, 31] and support the trailing-edge scattering hypothesis, in accordance with which the scattered hydrodynamic pressure waves are much more coherent in comparison with the pure isolated jet mixing noise. This effect is prevalent at low Mach numbers. In the case of the porous configurations, the coherence function shows a considerable reduction in the low-frequency range $St < 0.07$ compared to the baseline installed configuration, which is related to the reduced scattering noise effect for the porous trailing-edge.

It is important to note the sudden drop in coherence between the low-frequency spectral hump and the mid-frequency narrowband hump. This observation clearly indicates that the low-frequency spectral hump and the narrowband hump are driven by two different mechanisms. Previous studies [20, 21, 32] and aforementioned discussions have established that the low-frequency spectral hump results from the trailing-edge scattering. However, the narrowband peak is absent in some of the porous configurations and does not show dipolar behavior. Therefore, the narrowband peaks are not generated due to the trailing-edge scattering. This observation strengthens the suggested hypothesis that the narrowband hump is generated due to the acoustic feedback mechanism in the jet shear layer. Interestingly, the 80PPI case with the least porosity and permeability shows a notable reduction in coherence levels compared to the baseline and other porous configurations at the narrowband hump for all the tested Mach numbers. It can be recalled that the 80PPI porous treatment was earlier found to provide the best jet installation noise reduction capability (Fig. 10). This reconfirms a close connection between the jet installation noise reduction and the decline of the coherence function. Thereby, the suppression of the hydrodynamic waves scattered from the trailing-edge of the flat-plate by the porous treatments and their direct relation to the porosity and permeability of the trailing-edge.

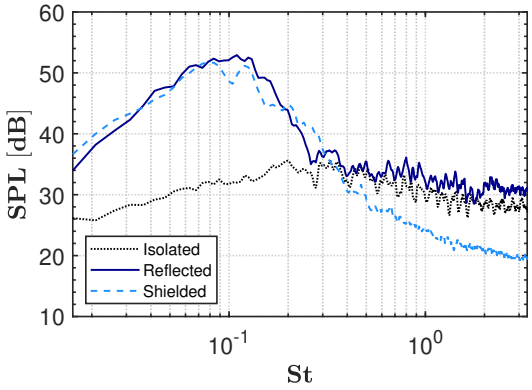

Figure 11: Sound pressure level on the shielded and reflected side for the baseline along with the isolated jet for $M = 0.3$ at $H = 2D$.

4.4. Velocity scaling

To further analyze the effect of the porous trailing-edge on the jet installation noise, the acoustic power scaling of the installed configurations, which is based on scaling the OASPL

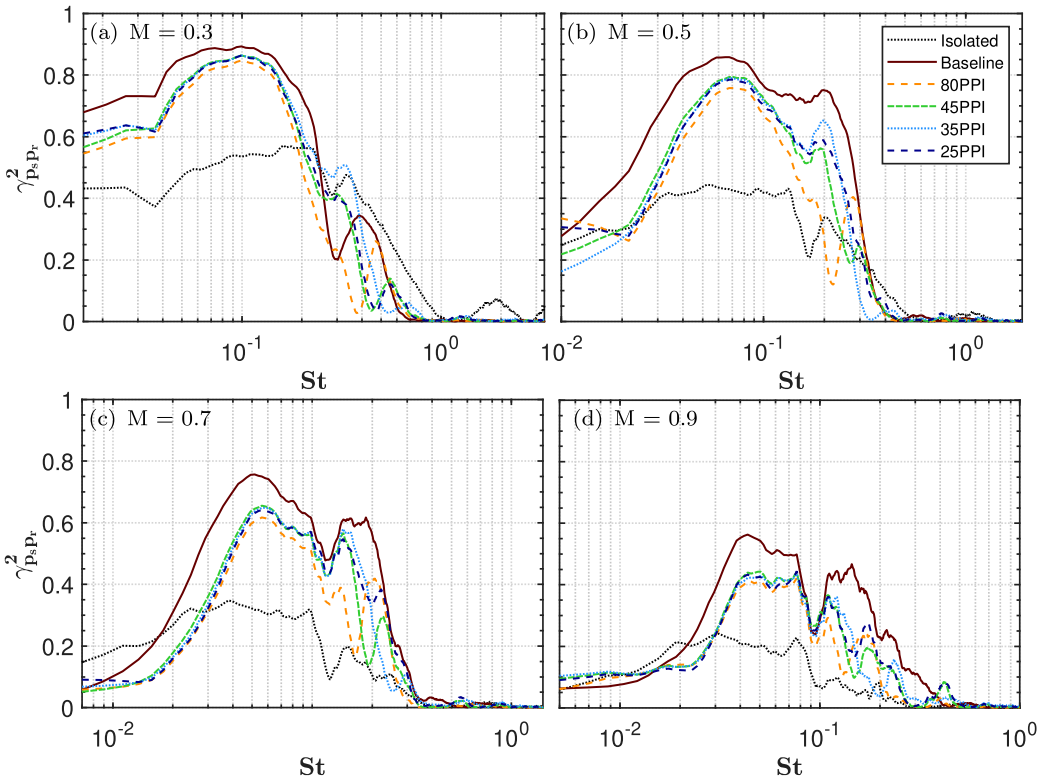

Figure 12: Coherence between shielded and reflected side for the installed and isolated jet for the baseline and porous configurations at different Mach numbers $M = 0.3 - 0.9$.

plots with the jet nozzle exit velocity is presented and discussed in this section for all the tested cases. In Fig. 13a, the results are first presented for inlet angle $\theta = 90°$ to be able to neglect the refraction effects thereby directly comparing with the Lighthill theory [36, 37]. This theory states that the far-field acoustic power of jet noise is proportional to the eighth power of the jet velocity at the nozzle exit, U_j^8, for cold jets at $\theta = 90°$. This was verified experimentally by several isolated jet noise studies [30, 38, 39]. The velocity scaling of the isolated jet from the present study is compared with Brown [40] in Fig. 13a. In excellent agreement with the theory, the jet noise from the present study scales with $U_j^{7.9}$ at $\theta = 90°$, in-line with previous experimental studies [20, 30, 38–40] for the isolated jets.

At the same time, the velocity scaling plot for installed jet in Figs. 13a and 14a for the baseline configuration shows a dipole-like scaling, U_j^6, as predicted for the case of high fluid loading on the surface [41]. A similar scaling law between U_j^5 and U_j^6 was also found in Brown [40] (see Fig. 13a) and in other previous experimental studies [2, 3, 42], in which a long flat-plate was used to study the jet installation effects. Experiments by Brown [40] and Lawrence et al. [42] demonstrated a velocity scaling close to U_j^5 for short surfaces and U_j^6 for longer surfaces. A transition region from U_j^5 to U_j^6 was documented by Lawrence et al. [42] when the surface extends downstream. In Fig. 13b, the results for the isolated and installed cases at upstream angle $\theta = 60°$ from the present study is compared with $\theta = 40°$ from the experiments by Rego et al. [20] from Delft University of Technology (TUD). Rego et al. [20] showed a scaling close to U_j^6 for the installed jet. The U_j^6 velocity scaling at $\theta = 60°$ from the present study for the installed configuration validates very well with the study by Rego

et al. [20] for upstream angles (see Fig. 13b).

The velocity scaling for different plate distances is shown in Fig. 14a. As the jet-plate distance increases, the effect of hydrodynamic pressure field scattering on the surface decreases, and thereby the velocity exponent n in U_j^n gradually increases towards $n = 8$. For example, at the furthest considered plate position $H = 4.5D$ the velocity scales at $U_j^{7.6}$. Figure 14b demonstrates the effect of the porous trailing-edge treatment on the velocity scaling for the same inlet angle $\theta = 90°$ at $H = 2D$. The baseline installed jet configuration scales in accordance with $U_j^{6.4}$ up to $M = 0.7$. At higher acoustic Mach numbers, the jet noise scales with a higher exponent. This is because for high jet velocities the noise generation mechanism is dominated by pure jet mixing noise, the scaling of which is governed by the Lighthill theory.

For the porous configurations at the low Mach number, the scaling exponent increases from $U_j^{6.4}$ to $U_j^{6.9}$. Furthermore, the porous treatment with the best noise reduction performance, 80PPI, has a higher slope, $U_j^{6.9}$ in comparison with the noisier, 25PPI configuration, which shows the scaling closer to U_j^6 typical of the dipole noise. The increased scaling exponent for the best performing porous configuration is attributed to the attenuation of the hydrodynamic pressure wave scattering achieved due to the use of the porous trailing surface. Again, at a higher Mach number, the baseline and the porous configurations follow similar scaling in accordance with the pure jet mixing noise. It must be noted that the scaling of $U_j^{6.9}$ for the 80PPI compares well with the study by Rego et al. [20], where the porous treatment showed a scaling of $U_j^{7.2}$ as shown in Fig. 13b. The slight difference in the scaling for porous configuration could be attributed to the difference in porosity and permeability.

The OASPL scaling with the jet velocity for different inlet angles is shown in Fig. 15. It can be noted that, due to the mean flow propagation effects, Lighthill's power law no longer holds well for inlet angles close to the jet axis in the flow direction even for isolated jets. At inlet angles towards the jet axis for the isolated jet, the velocity exponent n increases to U_j^9 in line with the previous studies [30, 38, 39, 43]. For higher inlet angles, the observed increased energy of jet noise is attributed to Lighthill's convective amplification which leads to very efficient noise propagation in a spreading jet flow at low frequencies corresponding to the peak jet noise [44]. The results for the velocity component n of the installed cases at $M = 0.3$ and 0.5 with and without porous treatment at high inlet angle $\theta = 150°$ follow the scaling similar to that of the isolated jet, U_j^9. For inlet angles $120 < \theta < 150°$, the velocity exponent for the installed configurations is lower than that for the isolated jet, while the noise levels of the baseline and porous cases have similar slopes. For these angles, the deviation from the U_j^8 law for the installed cases is due to a combination of the noise scattering at the trailing-edge and the mean flow propagation effects.

The velocity exponent calculated between $M = 0.3$ and 0.9 for different inlet angles, for the isolated and installed jets is shown in Fig. 16a. The slope coefficients obtained from the band-limited OASPL corresponding to the integration over $St = 0.02 - 3$ for the isolated jets show good agreement with the NASA data [30]. At lower inlet angles, $\theta < 100°$ the initial slope corresponds to about $U_j^{7.9}$, after which the velocity exponent gradually increases to U_j^9 at downstream locations closer to the jet axis. This observation is in-line with the previous studies [30, 38, 39] which have shown that the jet noise at inlet angles closer to the jet axis scales with U_j^9. For installed jet, studies [2, 3, 20, 40, 42] have shown dipole-like scaling with U_j^6 at upstream jet angles due to the scattering effects. For the baseline configuration with a solid trailing-edge, the velocity exponent in the scaling law increases from $U_j^{6.4}$ to $U_j^{7.4}$ over

the range of $\theta = 60° - 120°$. Over the same range of inlet angles, the porous configurations have an increased velocity exponent ranging from $U_j^{7.2}$ to $U_j^{7.4}$ with variations in the range of ± 0.1. This shows that the noise amplification due to the surface scattering ($\approx U_j^6$) is reduced for the porous configuration. The results in Fig. 16a demonstrate that the jet installation noise at large inlet angles ($\theta > 120°$) can be modeled using jet mixing scaling laws as the exponents compare well with the isolated jet. However, at lower inlet angles, the current analytical models used for isolated jets may not be directly applicable for installed jets.

To further analyze the effect of jet installation, the velocity exponent for different inlet angles is analyzed for a band-limited OASPL corresponding to the integration over the low-frequency hump representative of the jet installation effect, which is dominated by dipolar directivity ($St = 0.02 - 0.1$) in Fig. 16b. Notably, in this case, the velocity exponent coefficients for the installed configurations are close to $\approx U_j^5$, in agreement with the theoretical prediction for a perfectly rigid plate [41] and the previous NASA experiment by Brown [40]. For the porous configurations at higher inlet angles ($\theta = 100° - 120°$) the velocity exponent lies between U_j^6 and U_j^7. Notably, for inlet angles closer to the jet axis the slope increases from U_j^6 to U_j^9 where the noise is mainly dominated by pure turbulent jet mixing, and not due to the scattering at the surface trailing-edge. Overall, consistent with the previous sections, the above results clearly show that the application of porous materials reduces the effect of surface scattering of the near-field hydrodynamic pressure waves in comparison with the baseline installed jet configuration.

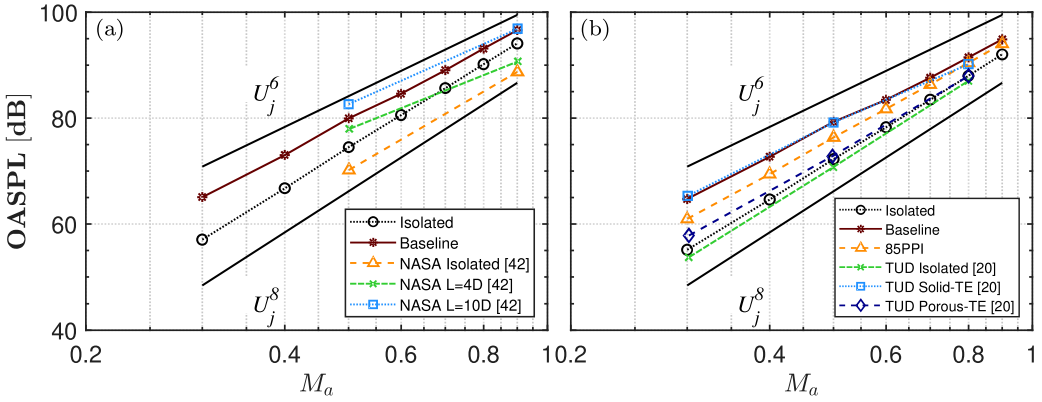

Figure 13: Scaling of Overall Sound Pressure Level with the jet acoustic Mach number for isolated and installed jet configurations (a) at $\theta = 90°$ compared with NASA study by Brown [40] and (b) at $\theta = 60°$ compared with TUD study by Rego et al. [20] .

4.5. Far-field pressure auto-correlation

It is often assumed that the radiated far-field pressure contains information on the noise source characteristics. The spectral and directional information from the far-field measurements could identify key characteristics linked directly to those of the noise sources. The auto-correlation could be used to gain not only valuable information on the spatial structure of the noise field in the radial and polar angle directions but also on the sources inside the jet [34]. The characteristic time scales of the far-field jet noise could be analyzed using the auto-correlation function. Previously, Tam et al. [34] used the auto-correlation of the far-field pressure signal to correlate the far-field noise with the effect of large and fine-scale turbulence

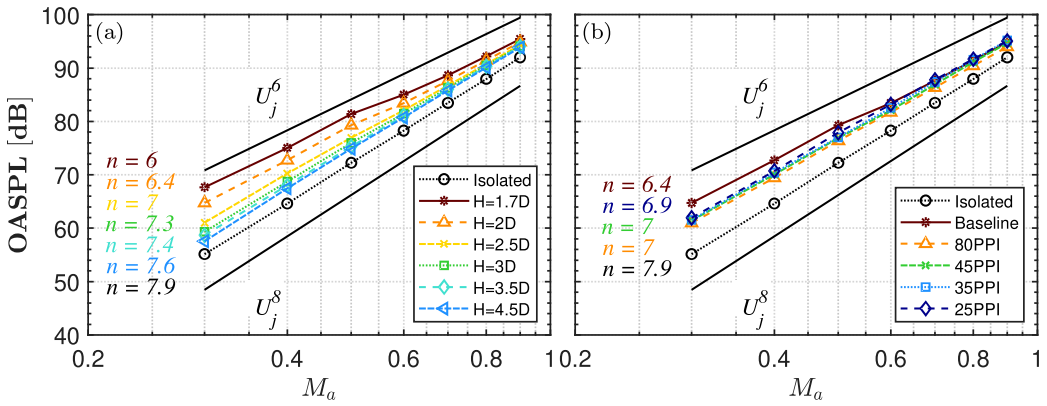

Figure 14: Scaling of Overall Sound Pressure Level at $\theta = 90°$ with the jet acoustic Mach number for isolated and installed jet configurations, (a) different plate positions for the Baseline case, and (b) tested porous trailing-edge configurations for plate distance $H = 2D$.

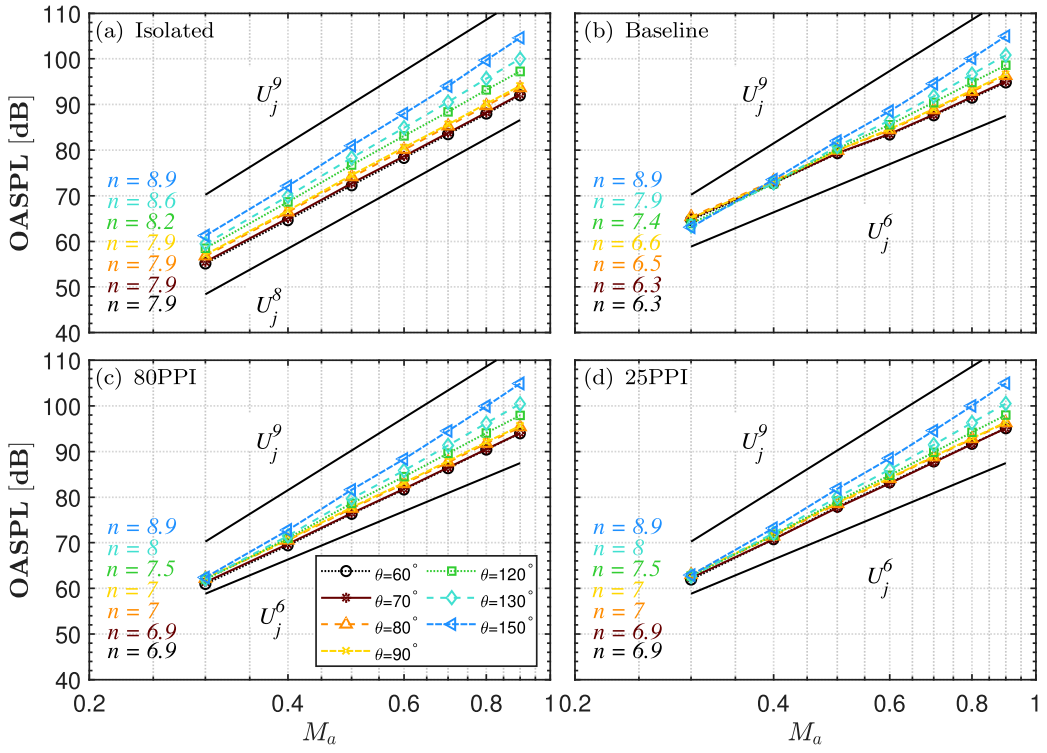

Figure 15: Scaling of Overall Sound Pressure Level with the jet acoustic Mach number for isolated and installed configurations at various inlet angles $\theta = 60° - 155°$ for a plate distance of $H = 2D$.

structures in the jet flow. At the same time, it can be noted that the far-field noise scales can be explicitly associated with the space and time scales of the auto-covariance of fluctuating turbulent Reynolds stresses in a cold subsonic jet. For a number of isolated jet flow cases, the growth of these structures in the shear layers of a spreading jet flow was analyzed computationally and experimentally using the Goldstein generalized acoustic analogy approach [45–48]. Notably, for isolated jets, the low-frequency noise sources, which correspond to the peak jet noise and large correlation scales, are typically located near the end of the

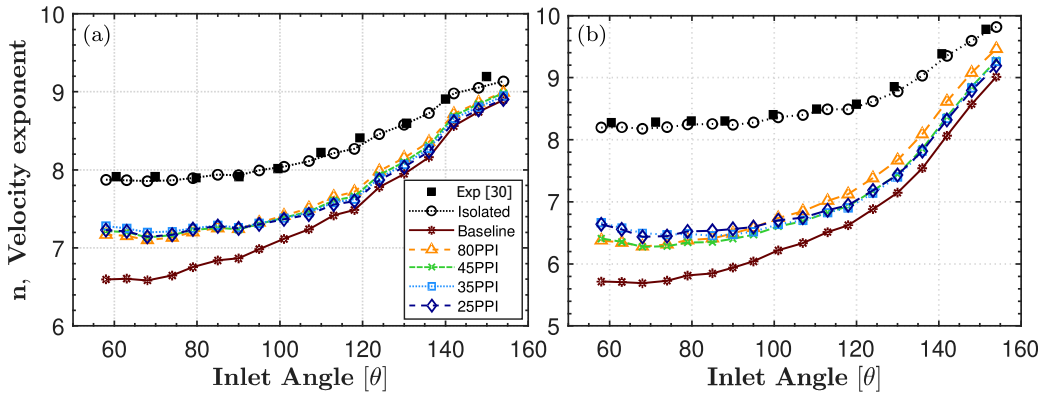

Figure 16: Velocity exponent for different inlet angles presented for all the tested configurations compared with isolated configuration of Brown and Bridges [30] (a) OASPL integrated over wide frequency range $St = 0.02 - 3$ (b) OASPL integrated over the low-frequency spectral hump $St < 0.1$.

jet potential core and predominantly radiate noise at shallow angles to the jet flow (at inlet angles $\theta > 120°$). At the same time, the small scales, which are related to high-frequency noise radiation can be attributed to the initial shear layer locations, and which mostly contribute to noise propagation at $\theta = 90°$ to the jet axis. The far-field pressure auto-correlation function used in the present study is defined as:

$$R_{p_r p_r}(\tau) = \frac{\overline{p_r(t+\tau)p_r(t)}}{p^2_{r_{rms}}}, \tag{2}$$

where p_r is the far-field pressure on the reflected side, $p_{r_{rms}}$ is the far-field pressure root-mean-squared, τ is the time delay and the time average is represented by the overbar. The auto-correlation coefficient $R_{p_r p_r}(\tau)$ is obtained by normalizing the auto-correlation function by the signal variance. The correlation coefficients indicate the similarity of the signals p_r at a given delay τ.

The results for the auto-correlation for the isolated and installed jet configurations at $M = 0.3, 0.5$ and 0.7 at four different inlet angles $\theta = 60°, 90°, 120°$ and $155°$ for a plate distance of $H = 2D$ are presented in Fig. 17. For the sake of brevity, the results for $M = 0.9$ are not presented as they were very similar to those for $M = 0.7$. The isolated jet clearly exhibits two distinct shapes of the auto-correlation function at $\theta = 60 - 90°$ corresponding to a small correlation scale and $\theta = 120°$ and $155°$ corresponding to a larger correlation scale, as previously observed by Tam et al. [34]. Following the previous discussion, the sharp auto-correlation shape in jets corresponds to energetic fine-scale turbulence structures representative of the jet's initial shear layer locations. At the same time, the large correlation scales represent the large turbulence structures located near the end of the jet potential core, which contribute to peak jet noise [49, 50]. The negative peaks in the auto-correlation function, which amplitude becomes very notable for the wide correlation functions corresponding to large correlation time scales, are due to the non-compactness effect of low-frequency jet noise sources.

The results for the low Mach number $M = 0.3$ in Fig. 17 demonstrate that the far-field pressure auto-correlation function for the isolated jet has a marginal widening for large inlet angles, in-line with the slow growth of the correlation time scale in the low Mach number jet,

which scale is proportional to the eddy convection velocity [7]. In comparison with this, the widening of the auto-correlation function for the installed jet cases indicates the presence of another noise mechanism that increases the coherence in comparison with pure jet mixing noise – the low-frequency noise amplification due to the scattered hydrodynamic waves. In comparison with the baseline installed jet configuration, both the width of the peak and the magnitude of the negative loops are reduced for the porous configurations, which is suggestive of the reduced jet installation effect as discussed in the previous sections.

As the jet Mach number is increased, the intensity of the negative trough reduces and the width of the correlations becomes progressively narrower for increasing jet velocities, which signifies the importance of jet mixing noise. For $M = 0.5$ and 0.7, at upstream and sideline inlet angles the width of the auto-correlation function of the baseline installed jet becomes only slightly larger than that of the porous configurations. Again, this suggests that for high Mach numbers the pure jet mixing noise effect becomes most dominant in comparison with the noise scattering at the trailing-edge.

Interestingly, the auto-correlation function of the 25PPI case exhibits mild oscillations at upstream and sideline inlet angles, which are related to the acoustic tones observed in the previous section. For the downstream locations, $\theta = 120°$ and $155°$ these oscillations are absent. The above observation is in line with the SPL results discussed in the previous sections, which showed that for high inlet angles the porous treatment effect was very small compared to both the baseline and the isolated jets at $M = 0.5$ and 0.7.

4.6. Influence of plate distance

The influence of jet-plate distance on the noise reduction effects of porous materials at 90° for $M = 0.3$ 0.5, 0.7, and 0.9 is analyzed in this section. Results of the SPL are presented for a fixed plate with a length of $L = 6.5D$, and various plate heights $H = 1.7D, 2D, 2.5D, 3D, 3.5D$, and $4.5D$ in Fig. 18. For the sake of brevity, the results are presented only for the baseline, 80PPI, and 25PPI. For $M = 0.3$, a spectral hump is observed in all the presented configurations in the low-frequency region due to the jet installation effect. Noise increase in the range of 15 dB can be found for the baseline configuration in the low frequencies as the plate distance is decreased from $H = 4.5D$ to $H = 1.7D$ for the baseline configuration. Similar trends are shown by the 80PPI and 25PPI configurations with noise increases ranging about ≈ 12 dB between the largest and smallest plate distance.

In comparison with the small Mach number case, a mild spectral hump is observed in the case of higher Mach numbers, $M = 0.5$ and 0.7, and noise increase in the range of ≈ 12 and ≈ 10 dB is found when decreasing the plate distance from $H = 4.5D$ to $1.7D$, respectively. For the porous configurations at $M = 0.5$ and 0.7, the difference in SPL between the largest and smallest plate distance reduces to $\approx$ 8dB and $\approx$ 5 dB, respectively. Therefore, it is evident that the jet installation noise more-or-less gradually increases as the plate height H decreases, which suggests the same trailing-edge noise mechanisms such as scattering with a dipole noise source are at play in all these cases. This is as expected since even the smallest plate distance, $H = 1.7D$ is still sufficiently large to preclude the direct interaction of the jet flow with the plate surface.

In the case of $M = 0.3$ with respect to the 80PPI and 25PPI configurations, a reduction of noise of about ≈ 6 dB and ≈ 3 dB for $H = 1.7D$, as opposed to the baseline configuration, is observed, respectively. However, when the plate distance is increased to $H = 4.5D$ there

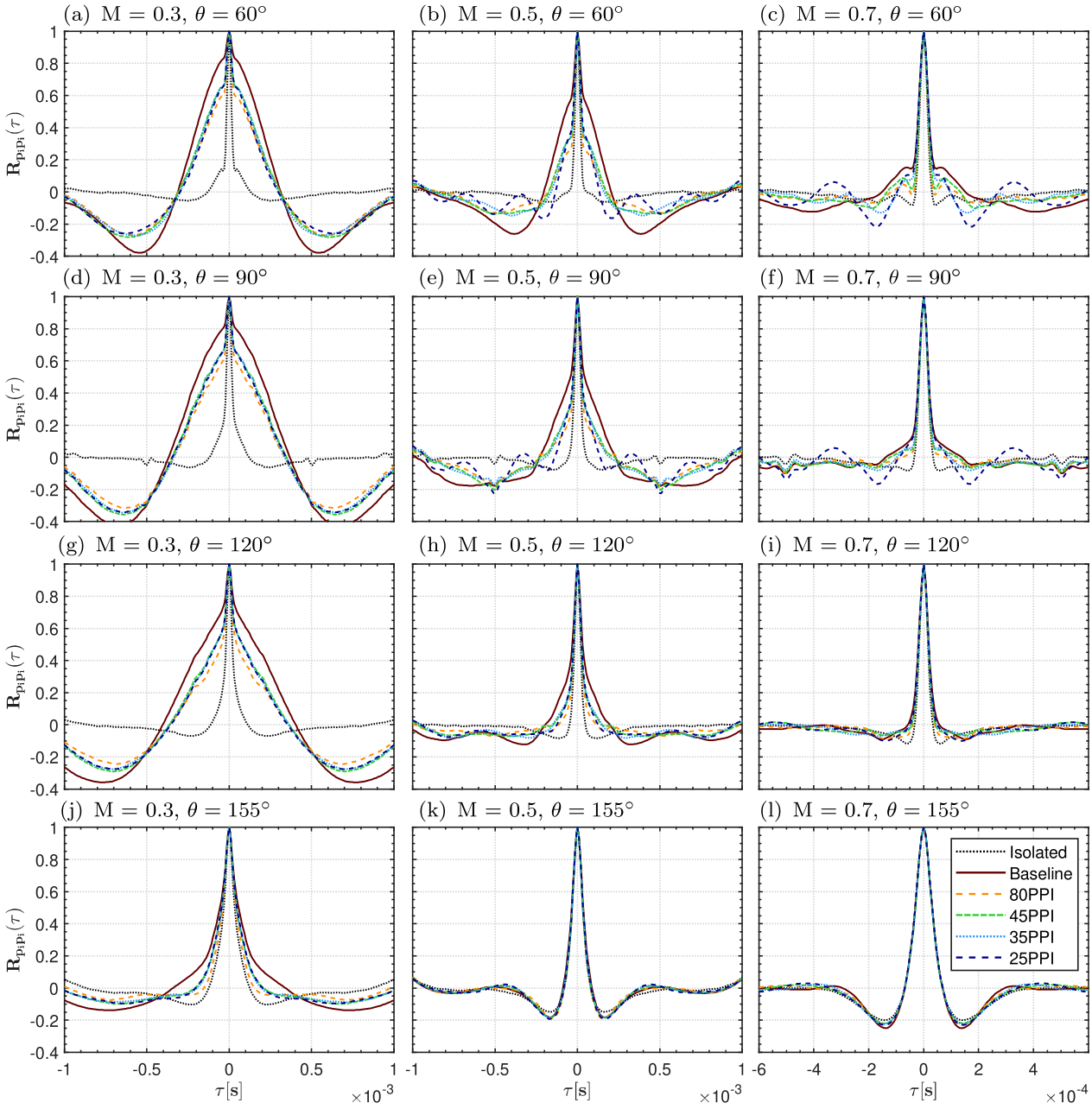

Figure 17: Auto-correlation of the far-field measurements for the isolated and installed configurations acquired at locations $\theta = 60°, 90°, 120°$ and $155°$ for $M = 0.3, 0.5$ and 0.7.

is little or no difference between the noise levels for all three configurations. Again, these observations confirm that the porous trailing-edges suppress the scattering effects of near-field pressure waves at the trailing-edge. It can also be noted that the mild narrowband hump observed in the baseline installed jet case at about $St = 0.3 - 0.4$ moves up in frequency to about $St = 0.3 - 0.45$ in the 80PPI configuration, which has the best noise reduction performance. Furthermore, this narrowband hump turns into two notable tones for the 25PPI configuration at $St = 0.35$ and $St = 0.45$, which were discussed in the previous sections. Moreover, the smallest plate height $H = 1.7D$ shows increased tonal magnitude compared

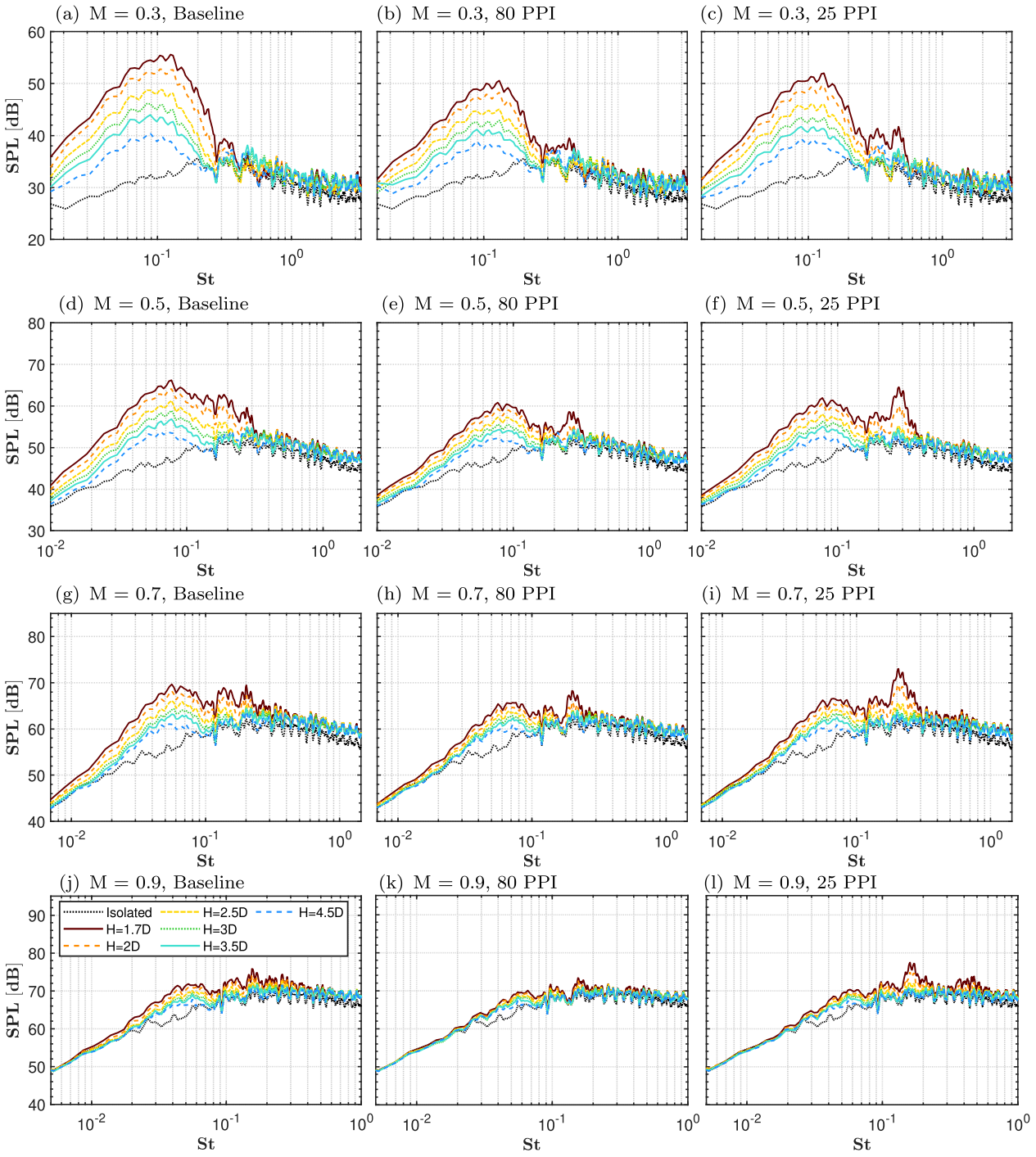

Figure 18: Sound pressure level for different plate distance for baseline, 80PPI and 25PPI at $\theta = 90°$ for $M = 0.3, 0.5, 0.7$ and 0.9.

to other plate heights for the 25PPI configuration. In addition, a significant increase in the narrowband hump ($St = 0.3 - 0.45$) can be observed for the 25PPI configuration compared to the baseline and 80PPI configurations. This strong narrowband hump for the 25PPI is persistent even at larger plate heights such as $H = 2D$. These observations strengthen

the hypothesis that the surface roughness and the junction between solid and flow-permeable surfaces might be triggering instabilities in the jet shear layer resulting in an acoustic feedback mechanism generating the tone. As the Mach number is increased to $M = 0.5$ and 0.7, the noise reductions of about $\approx$ 6 dB for 80PPI and $\approx$ 4 dB for 25PPI can be observed in comparison with the baseline configuration at $H = 1.7D$ whereas no difference is found at $H = 4.5D$ similar to the low Mach number cases. Interestingly, at $M = 0.9$ the narrowband hump that arises for the porous configurations has lower intensity compared to the baseline as opposed to the cases with lower Mach numbers. Since the narrowband hump is dominant at small plate distances $H = 1.7D - 2D$ and is absent for farther plate positions, it could also be hypothesized to be scrubbing noise in line with previous studies on porous trailing-edges in [26, 27]. However, further detailed studies at small plate distances along with near-field measurements are required to validate the suggested hypothesis.

The directivity pattern of the OASPL for various plate heights (H/D) are presented in Fig. 19. At first glance, the results clearly show a substantial increase in the OASPL for the baseline configuration at upstream angles $\theta < 90°$ for the smallest plate height of $H = 1.7D$ at low Mach number $M = 0.3$ compared to the isolated jet. As the plate is moved further away from the jet axis, the effects of jet installation reduce thereby reducing the OASPL magnitude substantially compared to the isolated jet. A difference in OASPL of about $\approx$ 2 dB at $H = 4.5$ was observed compared to $\approx$ 15 dB at $H = 1.7D$ relative to the isolated configuration. As previously discussed, this increase in shallow angles could be attributed to the scattering noise from the trailing-edge. As the Mach number is increased, the difference in OASPL between the plate heights decreases substantially, especially at small plate heights. For instance, at $M = 0.3$ the difference in OASPL between $H = 1.7D$ and $2D$ is $\approx$ 3 dB, whereas at $M = 0.9$ it is $<$ 1 dB. At low Mach numbers such as $M = 0.3$, the dipole noise source from the trailing-edge scattering is dominant and this can be seen from the increased OASPL at the directivity pattern at positions closer to the jet axis. The OASPL of the installed configurations at $\theta > 90°$ show an increase of about $\approx 5 - 7$ dB compared to the isolated configuration indicating that the trailing-edge noise source mechanisms are more dominant than that of the turbulence-mixing noise at low Mach numbers. This difference gradually decreases as the Mach number is increased, indicating that the turbulence-mixing noise becomes dominant at higher Mach numbers. Particularly, at $M = 0.9$ the difference between the installed and isolated configurations are almost absent at $\theta > 120°$. The general OASPL trend described thus far for the baseline configuration can also be observed for the porous treatments. From the directivity patterns of the OASPL, it is evident that the use of porous materials results in the reduction of the jet installation noise over a wide range of polar angles compared to the baseline configuration. Moreover, a key observation is the reduction in the OASPL between plate heights for the porous treatments. The difference in OASPL between plate heights $H = 1.7D$ and $2D$ is $\approx$ 3 dB for baseline, $\approx$ 1.8 dB for 80PPI and $\approx$ 2.5 dB for 25PPI at $M = 0.3$. This could be attributed to the varying scattering effects based on the porosity and permeability of the porous treatments at the trailing-edge. Some aspects of the differences could also be attributed to the narrowband humps and tones observed at small plate heights for the 25PPI configuration. These differences between porous treatments could be observed for the entire range of tested Mach numbers. Overall, the results show that the 80PPI configuration with the least porosity and permeability and with the least amount of surface roughness produces the best noise attenuation behavior for

jet installation effects for all the tested plate distances and Mach numbers.

It can be remarked that previous studies [15, 17, 21, 32] have shown that higher surface permeability may provide a better pressure balance between the upper and lower sides of the trailing-edge, thereby limiting the surface pressure fluctuations at low frequencies thus aiding with noise reduction. However, the current investigation does not fully support this observation. Indeed, the considered 80PPI configuration with a reduced permeability compared to the 25PPI configuration consistently showcases better performance with noise reduction for jet installation effects. Furthermore, it is hypothesized that the increased noise for the 25PPI case could be attributed to the acoustic feedback loop possibly triggered by the large surface roughness and junction noise between solid and flow-permeable porous treatment.

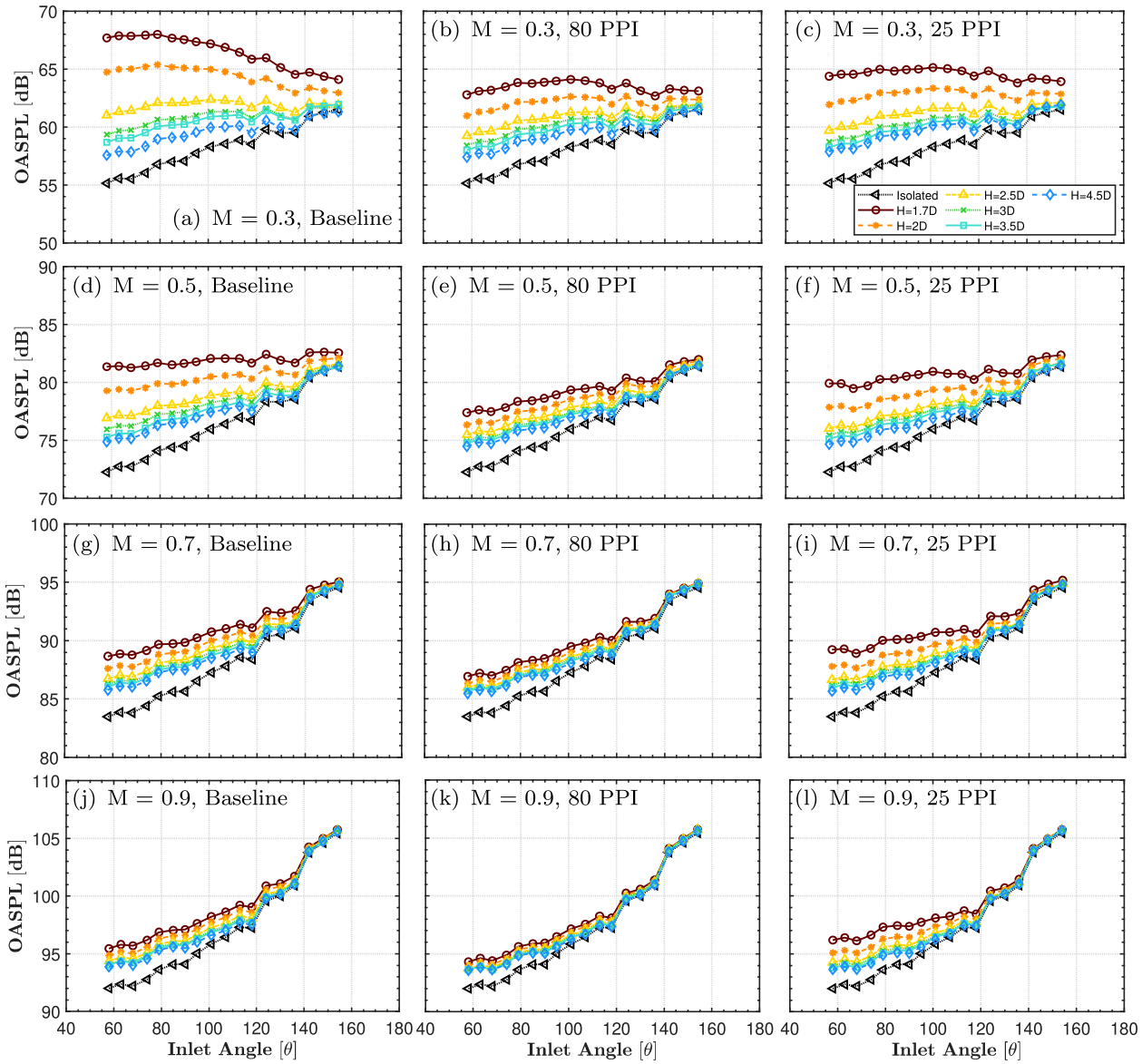

Figure 19: Overall sound pressure level for different plate distance for baseline, 80PPI and 25PPI at $\theta = 90°$ for $M = 0.3, 0.5, 0.7$ and 0.9.

5. Conclusion

A thorough experimental study was carried out in an anechoic chamber to demonstrate the noise reduction capabilities of porous trailing-edge treatment for installed jets using an unheated subsonic jet with a flat-plate placed at its vicinity. The interchangeable trailing-edge of the flat-plate was treated with four different types of porous metal foams with varying porosities, permeability, and surface roughness. Far-field noise measurements were taken at several directivity angles for a wide range of jet velocities. Noise reduction capabilities of the porous configurations were also assessed on the basis of plate distances. The noise results accurately showed the well-known characteristic spectral hump at low frequencies that arise due to the installation effects for the baseline line configuration with a solid trailing-edge. The spectral hump was very evident at low velocities where the noise spectra are dominated by the effects of jet installation. This increase can be associated with the combination of dipole sources on the surface and the quadrupole sources by turbulence mixing. A substantial reduction in the sound pressure levels was observed for the porous trailing-edges. Especially, the 80PPI configuration was relatively more efficient in reducing the installation noise than the other porous treatments. It is interesting to note that the 25PPI case with higher permeability than that of the 80PPI did not achieve better noise reduction performance. The 25PPI configuration gave rise to a strong tone at closer plate distances compared to the other tested porous cases. This is hypothesized to be due to the surface roughness or the junction noise between solid and flow-permeable 25PPI porous treatment triggering the acoustic feedback mechanism between the thin shear layers at the jet inlet, which is most susceptible to the linear hydrodynamic instability and the effective impedance condition of the trailing-edge. Coherence results showed a close connection between the installation noise reduction and the decline of the coherence function. Therefore noise reduction for the porous configurations could be owed to the suppression of the hydrodynamic waves scattered from the trailing-edge of the flat-plate. OASPL velocity scaling reconfirmed that the noise reduction of the porous configurations was related to the suppression of the scattering effects as it scaled close to U_j^5. In general, at close plate distances considerable increase in the noise levels was found in low to mid frequencies for jet installation cases. However, as the distance of the plate from the jet gradually increased, no changes were observed between the baseline and porous configurations. Therefore, it can be confirmed that the use of porous materials on the trailing-edge with potentially higher noise reduction capabilities is a viable solution for jet installation noise. Despite the noise reduction capabilities, the 25PPI porous material with the highest porosity and permeability gave rise to unfavorable tones which might affect the practical use of these materials. Previous studies [29] have shown that the porosity and permeability of the trailing-edge treatments affect the aerodynamic characteristics directly. However, the 80PPI case with the best noise reduction performance also produces the least drag compared to the 25PPI case [29]. Overall, further analysis on the effects of porosity and permeability of such materials is required as major differences in noise levels were found amongst the tested configurations. The effects of flow-permeable materials on the phenomenon of pressure imbalance must also be investigated in order to achieve better noise reduction since higher permeability always doesn't directly result in higher noise reduction as shown in this study.

Acknowledgement

The authors would like to acknowledge the Engineering and Physical Sciences Research Council (EPSRC) for supporting this research (Grant No. EP/S000917/1). The first author would like to acknowledge Dr. Xiao Liu for providing the CAD design for the aeroacoustic facility for the purpose of illustration. The first author would also like to acknowledge the phenomenal work done by Dr. Syamir Alihan S. A. on characterizing the porous material used in the present study.

References

[1] K. Bushell, Measurement and prediction of jet noise in flight, in: 2nd Aeroacoustics Conference, 1975, p. 461.

[2] R. Head, M. Fisher, Jet/surface interaction noise-analysis of farfield low frequency augmentations of jet noise due to the presence of a solid shield, in: 3rd aeroacoustics conference, 1976, p. 502.

[3] J. Lawrence, M. Azarpeyvand, R. Self, Interaction between a flat plate and a circular subsonic jet, in: 17th AIAA/CEAS aeroacoustics conference (32nd AIAA aeroacoustics conference), 2011, p. 2745.

[4] C. Brown, Jet-surface interaction test: far-field noise results, in: Turbo Expo: Power for Land, Sea, and Air, Vol. 44670, American Society of Mechanical Engineers, 2012, pp. 357–369.

[5] J. F. Williams, L. Hall, Aerodynamic sound generation by turbulent flow in the vicinity of a scattering half plane, Journal of fluid mechanics 40 (4) (1970) 657–670.

[6] I. V. Belyaev, G. A. Faranosov, N. N. Ostrikov, G. Paranin, A parametric experimental study of jet-flap interaction noise for a realistic small-scale swept wing model, in: 21st AIAA/CEAS Aeroacoustics Conference, 2015, p. 2690.

[7] V. A. Semiletov, S. A. Karabasov, Similarity scaling of jet noise sources for low-order jet noise modelling based on the goldstein generalised acoustic analogy, International Journal of Aeroacoustics 16 (6) (2017) 476–490.

[8] L. Rego, F. Avallone, D. Ragni, D. Casalino, Jet-installation noise and near-field characteristics of jet–surface interaction, Journal of Fluid Mechanics 895 (2020).

[9] P. Jordan, V. Jaunet, A. Towne, A. V. Cavalieri, T. Colonius, O. Schmidt, A. Agarwal, Jet–flap interaction tones, Journal of Fluid Mechanics 853 (2018) 333–358.

[10] C. K. Tam, S. Chandramouli, Jet-plate interaction tones relevant to over-the-wing engine mount concept, Journal of Sound and Vibration (2020) 115378.

[11] B. Lyu, A. P. Dowling, Modelling installed jet noise due to the scattering of jet instability waves by swept wings, Journal of Fluid Mechanics 870 (2019) 760–783.

[12] D. Casalino, A. Hazir, Lattice boltzmann based aeroacoustic simulation of turbofan noise installation effects, in: 23rd International Congress on Sound and Vibration, 2014, pp. 1–8.

[13] C. Hughes, The promise and challenges of ultra high bypass ratio engine technology and integration (2011).

[14] V. Mengle, R. Elkoby, L. Brusniak, R. Thomas, Reducing propulsion airframe aeroacoustic interactions with uniquely tailored chevrons: 1. isolated nozzles, in: 12th AIAA/CEAS Aeroacoustics Conference (27th AIAA Aeroacoustics Conference), 2006, p. 2467.

[15] E. Sarradj, T. Geyer, Noise generation by porous airfoils, in: 13th AIAA/CEAS Aeroacoustics Conference (28th AIAA Aeroacoustics Conference), 2007, p. 3719.

[16] M. Herr, K.-S. Rossignol, J. Delfs, N. Lippitz, M. Mößner, Specification of porous materials for low-noise trailing-edge applications, in: 20th AIAA/CEAS aeroacoustics conference, 2014, p. 3041.

[17] J. Revell, J. Revell, H. Kuntz, F. Balena, C. Horne, B. Storms, R. Dougherty, H. Kuntz, F. Balena, C. Horne, et al., Trailing-edge flap noise reduction by porous acoustic treatment, in: 3rd AIAA/CEAS aeroacoustics conference, 1997, p. 1646.

[18] R. C. Alejandro, M. M. Roberto, A. Francesco, R. Daniele, S. Mirjam, v. d. Z. Sybrand, Broadband trailing-edge noise reduction using permeable metal foams, in: INTER-NOISE and NOISE-CON Congress and Conference Proceedings, Vol. 255, Institute of Noise Control Engineering, 2017, pp. 2755–2765.

[19] A. R. Carpio, R. M. Martinez, F. Avallone, D. Ragni, M. Snellen, S. van der Zwaag, Experimental characterization of the turbulent boundary layer over a porous trailing edge for noise abatement, Journal of Sound and Vibration 443 (2019) 537–558.

[20] L. Rego, D. Ragni, F. Avallone, D. Casalino, R. Zamponi, C. Schram, Jet-installation noise reduction with flow-permeable materials, Journal of Sound and Vibration 498 (2021) 115959.

[21] L. Rego, F. Avallone, D. Ragni, D. Casalino, On the mechanisms of jet-installation noise reduction with flow-permeable trailing edges, Journal of Sound and Vibration (2021) 116582.

[22] Y. D. Mayer, H. K. Jawahar, M. Szőke, S. A. S. Ali, M. Azarpeyvand, Design and performance of an aeroacoustic wind tunnel facility at the university of bristol, Applied Acoustics 155 (2019) 358–370.

[23] J. Bridges, C. Brown, Parametric testing of chevrons on single flow hot jets, in: 10th AIAA/CEAS aeroacoustics conference, 2004, p. 2824.

[24] H. E. Bass, L. C. Sutherland, A. J. Zuckerwar, D. T. Blackstock, D. Hester, Atmospheric absorption of sound: Further developments, The Journal of the Acoustical Society of America 97 (1) (1995) 680–683.

[25] H. Bass, L. Sutherland, A. Zuckerwar, D. Blackstock, D. Hester, Erratum: atmospheric absorption of sound: further developments [j. acoust. soc. am. 97, 680–683 (1995)], The Journal of the Acoustical Society of America 99 (2) (1996) 1259–1259.

[26] S. A. Showkat Ali, M. Azarpeyvand, C. R. I. da Silva, Trailing-edge flow and noise control using porous treatments, Journal of Fluid Mechanics 850 (2018) 83–119.

[27] S. A. Showkat Ali, M. Azarpeyvand, C. R. I. da Silva, Trailing edge bluntness noise reduction using porous treatments, Journal of Sound and Vibration 474 (2020) 115257.

[28] S. A. Showkat Ali, M. Azarpeyvand, M. Szőke, C. R. Ilário da Silva, Boundary layer flow interaction with a permeable wall, Physics of Fluids 30 (8) (2018) 085111.

[29] S. A. Showkat Ali, Flow over and past porous surfaces, Ph.D. thesis, University of Bristol (2018).

[30] C. Brown, J. Bridges, Small hot jet acoustic rig validation, Technical Report NASA NASA/TM—2006-214234 (2006).

[31] A. V. Cavalieri, P. Jordan, W. R. Wolf, Y. Gervais, Scattering of wavepackets by a flat plate in the vicinity of a turbulent jet, Journal of sound and Vibration 333 (24) (2014) 6516–6531.

[32] L. Rego, F. Avallone, D. Ragni, D. Casalino, Jet-installation noise and near-field characteristics of jet–surface interaction, Journal of Fluid Mechanics 895 (2020).

[33] J. F. Williams, L. Hall, Aerodynamic sound generation by turbulent flow in the vicinity of a scattering half plane, Journal of fluid mechanics 40 (4) (1970) 657–670.

[34] C. K. Tam, K. Viswanathan, K. Ahuja, J. Panda, The sources of jet noise: experimental evidence, Journal of Fluid Mechanics 615 (2008) 253–292.

[35] C. Mead, P. Strange, Under-wing installation effects on jet noise at sideline, in: 4th AIAA/CEAS Aeroacoustics Conference, 1998, p. 2207.

[36] M. J. Lighthill, On sound generated aerodynamically i. general theory, Proceedings of the Royal Society of London. Series A. Mathematical and Physical Sciences 211 (1107) (1952) 564–587.

[37] M. J. Lighthill, On sound generated aerodynamically ii. turbulence as a source of sound, Proceedings of the Royal Society of London. Series A. Mathematical and Physical Sciences 222 (1148) (1954) 1–32.

[38] A. Khavaran, J. Bridges, Shjar jet noise data and power spectral laws, Tech. rep., NASA TM-2009-215608 (2009).

[39] C. Bailly, C. Bogey, T. Castelain, Subsonic and supersonic jet mixing noise—in measurement, Simulation and control of subsonic and supersonic jet noise. von Karman Institute for Fluid Dynamics (2016).

[40] C. A. Brown, Jet-surface interaction test: far-field noise results, Journal of Engineering for Gas Turbines and Power 135 (7) (2013).

[41] N. Curle, The influence of solid boundaries upon aerodynamic sound, Proceedings of the Royal Society of London. Series A. Mathematical and Physical Sciences 231 (1187) (1955) 505–514.

[42] J. Lawrence, Aeroacoustic interactions of installed subsonic round jets, Ph.D. thesis, University of Southampton (2014).

[43] A. R. Proenca, Aeroacoustics of isolated and installed jets under static and in-flight conditions, Ph.D. thesis, University of Southampton (2018).

[44] M. Goldstein, A. Sescu, M. Afsar, Effect of non-parallel mean flow on the green's function for predicting the low-frequency sound from turbulent air jets, Journal of fluid mechanics 695 (2012) 199–234.

[45] M. E. Goldstein, A generalized acoustic analogy, Journal of Fluid Mechanics 488 (2003) 315–333.

[46] M. Harper-Bourne, Jet noise turbulence measurements, in: 9th AIAA/CEAS aeroacoustics conference and exhibit, 2003, p. 3214.

[47] S. Karabasov, C. Bogey, T. Hynes, An investigation of the mechanisms of sound generation in initially laminar subsonic jets using the goldstein acoustic analogy, Journal of Fluid Mechanics 714 (2013) 24–57.

[48] V. A. Semiletov, S. A. Karabasov, A volume integral implementation of the goldstein generalised acoustic analogy for unsteady flow simulations, Journal of Fluid Mechanics 853 (2018) 461–487.

[49] B. M. Harker, K. L. Gee, T. B. Neilsen, A. T. Wall, S. A. McInerny, M. M. James, On autocorrelation analysis of jet noise, The Journal of the Acoustical Society of America 133 (6) (2013) EL458–EL464.

[50] B. M. Harker, T. B. Neilsen, K. L. Gee, A. T. Wall, M. M. James, Spatiotemporal-correlation analysis of jet noise from a high-performance military aircraft, AIAA Journal 54 (5) (2016) 1554–1566.